Supplementary Information: Spatiotemporal dynamics of synthetic microbial consortia in microfluidic devices

Razan N. Alnahhas,[†] James J. Winkle,[†] Andrew J. Hirning,[†] Bhargav Karamched,[‡] William Ott,[‡] Krešimir Josić,[‡,¶,†] and Matthew R. Bennett[*,†,§]

[†]*Department of BioSciences, Rice University, Houston, TX, USA*

[‡]*Department of Mathematics, University of Houston, Houston, TX, USA*

[¶]*Department of Biology and Biochemistry, University of Houston, Houston, TX, USA*

[§]*Department of Bioengineering, Rice University, Houston, TX, USA*

E-mail: matthew.bennett@rice.edu

Strain Bands, Cell Seeding, and Interface Simulation Model

To characterize the expected number of strain bands in experiments that used the open-walled microfluidic device, we created a sequential coin-flipping model for the initial seed strain type and placement of cells. Our goal was to create as simple a model as possible that captures the correlation between the number of cells seeded in an experiment and the number of resulting strain bands. We also developed a strain-interface simulation model where each interface from the coin-flipping model performs a random walk at a fixed rate in order to capture the strain ratio fluctuations observed in experiments. Details of the models follow below.

Seed cell and band formation modeling

To simulate loading of cells in the trap, our model flips a fair coin to choose one of two strains and places the seed cell along the centerline, where we assume a one-dimensional reduction of the initial seed positions in the trap. After cell loading, we assume initial seed cells grow symmetrically until making contact with another growing seed cell colony; at which time, if the two colonies are of different strain types, the merged colony forms a strainA-strainB interface. The colonies in this way continue to expand (possibly forming other interfaces with other single or merged colonies) until the trap fills (details of the strain-interface simulation algorithm for trap filling is given below). We also assume that a full trap results in vertical, single cell-width columns, where the identity of each column is of strain type 'A' or 'B' (in the experimental data these were sender or receiver cells) and that each column is derived directly from an initial seed cell colony. Cells are thus modeled as being initialized along the centerline of the trap and then being grown laterally and uniformly until the trap consists completely of side-by-side columns. Our model is reductive and does not capture the full complexity of the two-dimensional trap geometry and dynamics of trap filling (for example, seed cells will not always be located near the centerline of the trap and complex hydrodynamic effects can lead to shifting of cells bands during trap filling). However, we use our model in Fig. 5 in the main text, which shows good agreement between the number of seeded cells and the initial number of bands formed as measured in the experiments.

In this model, we are interested in the expected number of *bands* of cells vs. the number of cells seeded, where a band is a contiguous group of columns, all of the same strain type. The number of initial bands in an experiment is determined by the number of strainA-strainB interfaces that form during the colonies' expansion phase after cell seeding. In our model, the number of bands is determined by the number of transitions from one strain type to the other ('A' to 'B' or vice versa) in the initial coin-flipping initialization of seed cells. Since our model restricts cells to grow uniformly and laterally, no additional bands are generated after seeding in our one-dimensional reduction (but the width of each band increases uniformly

for each band to model cell proliferation up to trap filling).

Let n be the number of seed cells (seeded with equal probability 0.5 of each strain type) and let b represent the number of resulting bands. The probability distribution of bands b as a function of seed cell count n follows a binomial distribution with the inclusion of one initial success trial. Here, a "success" is defined as the creation of an additional cell band upon seeding an additional cell (a "trial") and results from a trial where the strain type changes from that of the previous trial. To account for the first seed cell forming the first band, we begin with one success with the first trial. The number of Bernoulli trials is then $n-1$ after the initial strain is placed to form the first band and the probability of the next success is $p = 0.5$ (unbiased probability for each strain) for each successive trial. Our modified binomial distribution of resulting bands for $n \geq 1$ trials (seed cells) is then:

$$Pr(b, n, 0.5) = \begin{cases} 0, & \text{for } b = 0; \\ \binom{n-1}{b-1} \cdot (0.5)^{n-1}, & \text{for } b = 1, 2, ..., n. \end{cases} \tag{1}$$

The expectation and variance of the number of bands is:

$$\mathbb{E}[b] = \frac{n+1}{2} \qquad \mathbf{var}(b) = \frac{n-1}{4}. \tag{2}$$

In Fig. 5, we used a range of ± 3 standard deviations from the mean of this distribution for each number of initial seed cells to compare to the experimentally reported band count.

Strain-interface simulations to model strain ratio dynamics

Using the above cell seeding construction, we wanted to investigate the dynamics of strain fraction fluctuations by extending the model to include a birth/death spatial invasion process at the interfaces of the bands. The fraction of one strain in the population in experiments is computed by pixel counts of a fluorescent image (e.g., yfp) relative to the total pixel count of the entire image within the trap boundary. Strain fraction is, however, spatially correlated

since bacteria grow axially and tend to form columns of the same strain lineage as cells proliferate (see further discussion of this assumption below). As above, our model assumes a one-dimensional reduction of the bacterial population such that an idealized column of cells is then represented by a single cell along the centerline of the trap.

In the main text, we report a correlation between the measured temporal instability of the population fraction of one of the strains (measured using the strain fraction range over the experiment) and the number of initial strain bands formed. We wanted to use our model to investigate invasion rates across the band interfaces to see if this could account for the measured temporal variation and correlation with the initial number of bands. Thus, we extended our model to include a birth/death process at the strain band interfaces such that at a fixed rate and for all interfaces, one band (chosen with equal probability) of each interface grew by a Poisson-distributed number of cells and deleted an equivalent number of cells from the other band, thus keeping the total cell count constant. We thus performed a random walk (using a mean 1 Poisson-distributed step size) of each interface position; this generated a time series for the resulting strain fraction from which we measured the resulting strain fraction range over a single simulation and computed its mean and standard deviation over 10,000 simulation runs. In some cases a band would become extinct, which resulted in combining the two adjacent bands and in reducing the total band count by two (if in the bulk) or by one (if on the edge). If the population then became fixed by one strain of the population, the simulation run was terminated.

In order to keep our model as simple as possible and to avoid over-fitting, we used a single rate parameter to fit our model to the experimental strain fraction range data reported in the main text. We defined a rate parameter X that represents the number of interaction events per interface per experimental hour. We found that setting $X = 4$ gave good trend agreement between simulations and experiments (see Fig. S10) and we set this parameter by matching the mean strain ratio range for the smallest size trap. This parameter is meant to capture stochastic interactions between cells that occur in the course of an experiment

that lead to changes in strain composition in a local area of the trap (further discussion given below). We believe this parameter is physically grounded since cell division time in exponential phase and in rich media of the experiments is $\approx 20 - 30$ minutes. Thus, at a thirty minute division time, for example, we expect (on average) 2 division events each experimental hour for each side of a strainA-strainB interface at an idealized mother-cell position and that division events are a likely cause of cell-folding that can lead to lateral invasion across strains. Although this is an over-simplified model of the role of cell division in stochastic interactions between strains, we are motivated to keep the model simple in order to investigate how it scales with trap size and the number of seed cells.

In our one-dimensional model, a single cell position represents a fixed fraction of the cell population and replacement of one strain by another alters the strain ratio (we only simulate interactions at an interface between strains since we do not model mutations between strains). We used a Poisson distribution of mean 1 for the invasion depth to include both non-invasive interactions and interactions with a lateral reach greater than one cell width in each simulation step. The invasion depth was sampled for each interface and for each interaction time step independently.

The algorithm for our simulation is as follows:

1. **Input**: (set from experimental data) width of trap in microns w, number of seed cells n, simulation time T (hours); (free model parameter) interaction rate parameter X

2. Perform coin-flipping sequence n times to generate the initial band structure and record the initial number of bands b.

3. Proliferate each seed cell by doubling until the population size first exceeds the width of the trap (we assume each cell is one micron wide). To reduce the population size to w, remove one cell sequentially from each band, removing a band if its cell count goes to zero and merging flanking bands (if not an edge band). This completes the initialization stage.

4. **Main loop:** Sequentially for each interior band interface, randomly choose an invasion direction and add (subtract) a mean 1 Poisson random number of cells to (from) the invading (invaded) band. Remove and merge bands if a band cell count reaches zero as necessary. Compute and record the resulting strain fraction to generate the time series.

5. Iterate the sequential band interface birth/death process (interacting all interfaces in each iteration) X times to complete one hour of simulated experimental wall time and continue for T hours of iterations.

6. Repeat each simulation 10,000 times and generate statistical data for initial stripe distribution, (vs. number of seeded cells), strain fraction range ($max - min$) and standard deviation across simulation runs.

In Fig. S10 we show the result of 10,000 simulation runs for the 5 different experimental trap widths using seed cell counts that resulted in the average number of bands (see expectation formula, above) as reported for each trap size in the first five panels of Fig. S11. We used a simulation time of 20 hours, which approximates that in the experiments. In Fig. S11 (bottom-right panel) we compare the simulated strain ratio range while varying the number of seed cells in the 2000 µm length trap, which captures the increased strain fraction variability with increasing number of seed cells, as reported in the main text.

Modeling discussion

Our simulation model captures two principal trends reported from our experiments of two-strain consortia in the open-walled microfluidic device: (1) Increasing the trap width *decreases* the expected strain fraction variation (as measured by its experimental range), and (2) increasing the number of seeded cells *increases* this variation for a fixed trap size. Our model is, however, an over-simplification in many respects and does not capture behaviors that may also contribute to population dynamics in our two-strain experiments. Experimen-

tal data clearly show, for example, that cells do not form perfect columns (as assumed in our one-dimensional reduction) and may move laterally due to hydrodynamic effects (due to media flow in the flanking channels) or cell blockage (lower-height irregularities of the trapping region and/or larger than average cell diameter). Such effects could account for the differences seen in the larger-width trap experiments and simulations (with our fitting, simulations showed a lower than experimentally reported strain fraction range for the larger devices), but further investigation would be required to fully support this claim (for example using high frame-rate image capture, lineage tracking, and hydrodynamic media flow models). We believe that a Poisson distribution for the invasion depth for each interface interaction partially captures these experimental effects, but our simulations suggest that their severity may scale with increasing trap size, though properly attributing all sources is difficult without more precise models.

Our one-dimensional model is based on the emergent spatial correlations that result from axial growth of bacteria in the close-packed environment of the microfluidic trap. In contrast, our model would not be appropriate for bacterial cells in a low density environment where, for example, run-and-tumble behaviors dominate cell motion and one may expect a diffusive model to be more appropriate for strain interactions. Although "mother-cell positions" (cell-pole positions that determine the strain type in local regions of the trap, see main text) are frequently not centered in the trap and can shift position due to the stochastic lateral-motion influences mentioned above, their progeny still generate strong spatial correlations from proliferation and formation of quasi-columnar cell flows. Thus, mother-cell positions account for the strain identity of an entire lineage of cells on some spatial and temporal scale and although such lineages fluctuate in size (due to channel removal and secondary lateral mixing), an invasion of a mother-cell position due to stochastic fluctuations of the two strains leads to flushing of the previous lineage locally. Full accounting of the causal chain for cells exiting the trap is challenging and computationally costly and our one-dimensional reduction attempts to simplify the modeling while still capturing the experimentally observed corre-

lations. We conclude that the number of strain-interfaces and the rate of their interactions with stochastic local invasion of mother-cell positions can account for the trends we see in the experimental data. However, experimental environments in microfluidic traps are subject to many sources of noise that are difficult to predict or control. When employing cell-cell signaling in consortial experiments, one wants to keep the density of strain interfaces high to improve coupling between strains. However, our data and modeling suggest that increasing the number of such interfaces can increase the temporal instability of the strain ratio, which is also of concern both locally and globally, in order to balance functional and spatial distribution of the strains in a multi-strain experiment.

Diffusion Model

Let $x \in \mathbb{R}^+ \equiv [0, \infty)$. Partiton $\mathbb{R}^+$ into two subsets I_1, I_2, where $I_1 = [0, L_s]$ and $I_2 = (L_s, \infty)$. I_1 will correspond to the region where we have a densely packed sender strain. Hence, L_s represents the thickness of the stripe formed by these sender cells. I_2 will be the region where receiver cells, for example, may exist. We are interested in understanding the density of a chemical signal U produced by the sender strain uniformly in I_1 at a point that is a distance δ away from the right endpoint of I_1 (i.e. a distance δ from the stripe of sender cells) as a function of the thickness of the stripe, L_s. Let $u_1(x,t)$ denote the density of chemical U at a point x at time t in I_1. Let u_2 describe the corresponding density in I_2. The following are the dynamics for u_1, u_2:

$$\frac{\partial u_1}{\partial t} = \alpha + D\frac{\partial^2 u_1}{\partial x^2} - \gamma u_1, \quad x \in I_1 \tag{3}$$

$$\frac{\partial u_2}{\partial t} = D\frac{\partial^2 u_2}{\partial x^2} - \gamma u_2, \quad x \in I_2 \tag{4}$$

The signal diffuses and degrades at a rate γ in all of $\mathbb{R}^+$ but in I_1 the signal is produced at some rate α. This is what is captured in these equations. We note that γ represents a degradation in a loose sense. Most likely this rate will represent a rate of absorption or

consumption of the signal molecule. The boundary conditions are:

$$\frac{\partial u_1}{\partial x}\Big|_{x=0} = 0$$
$$\lim_{x\to\infty} u_2 = 0$$
$$u_1(L_s, t) = u_2(L_s, t)$$
$$\frac{\partial u_1}{\partial x} = \frac{\partial u_2}{\partial x}\Big|_{x=L_s}$$

The first boundary condition says none of the chemical exits from the boundary at $x = 0$. The second boundary condition keeps the solutions physical by preventing blowup. The last two boundary conditions impose continuity in the density and first derivative of the density at the partitioning point $x = L_s$. Examining this system at steady state and imposing the first two boundary conditions, we obtain

$$u_1(x) = 2A\cosh\left(x\sqrt{\frac{\gamma}{D}}\right) + \frac{\alpha}{\gamma} \tag{5}$$
$$u_2(x) = Be^{-x\sqrt{\frac{\gamma}{D}}} \tag{6}$$

The last step is to impose continuity at $x = L_s$. In doing this, we obtain the linear system

$$\mathbf{Av} = \mathbf{b},$$

where

$$\mathbf{A} = \begin{bmatrix} 2\cosh\left(L_s\sqrt{\frac{\gamma}{D}}\right) & e^{-L_s\sqrt{\frac{\gamma}{D}}} \\ 2\sinh\left(L_s\sqrt{\frac{\gamma}{D}}\right) & e^{-L_s\sqrt{\frac{\gamma}{D}}} \end{bmatrix}, \mathbf{v} = \begin{bmatrix} A \\ B \end{bmatrix}, \mathbf{b} = \begin{bmatrix} -\frac{\alpha}{\gamma} \\ 0 \end{bmatrix}$$

We now plot $u_2(L_s + \delta)$ as a function of L_s. We can also plot the density profile of the chemical signal $u(x)$. It is also straightforward to generalize the above framework to the case where there are receiver cells on either side of the region where sender cells are densely packed. In this case, we let our domain be all of $\mathbb{R}$ and partition it into I_1, I_2, I_3, where

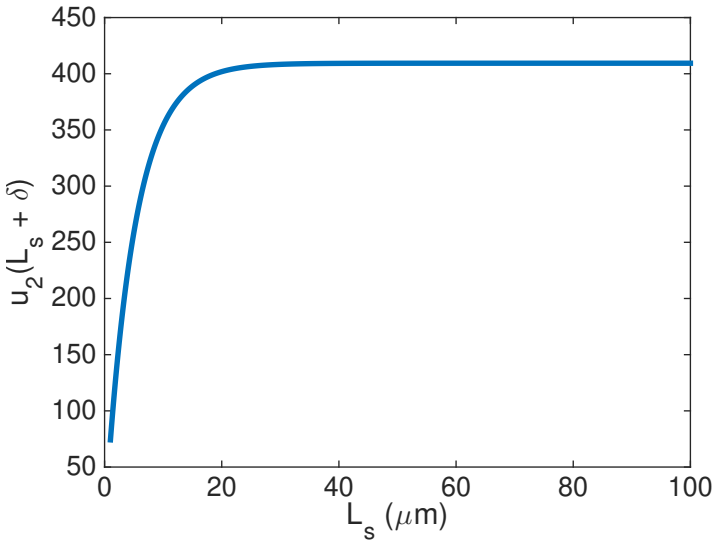

Figure S1: Plot of $u_2(L_s + \delta)$ as a function of L_s. Parameter values are $D = 1$, $\gamma = 0.01$, $\delta = 2$, and $\alpha = 10$.

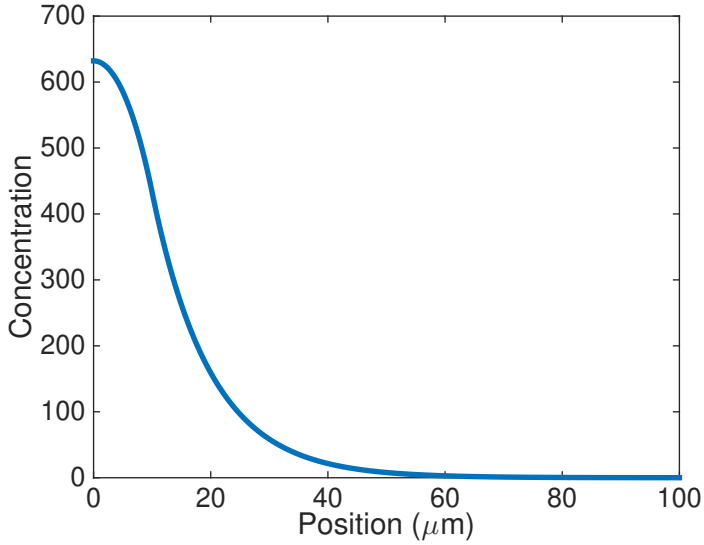

Figure S2: Plot of $u(x)$. Parameter values are $D = 1$, $\gamma = 0.01$, $L_s = 10$, and $\alpha = 10$.

$I_1 = (-\infty, -L_s/2)$, $I_2 = [-L_s/2, L_s/2]$, and $I_3 = (L_s/2, \infty)$. We let $u_i(x,t)$ be the density of chemical U in the set I_i, for $i = 1, 2, 3$. We impose zero conditions at $x = \pm\infty$ and continuity conditions analogous to the above case at $x = \pm\frac{L_s}{2}$.

$$\frac{\partial u_1}{\partial t} = D\frac{\partial^2 u_1}{\partial x^2} - \gamma u_1, \quad x \in I_1 \tag{7}$$

$$\frac{\partial u_2}{\partial t} = \alpha + D\frac{\partial^2 u_2}{\partial x^2} - \gamma u_2, \quad x \in I_2 \tag{8}$$

$$\frac{\partial u_3}{\partial t} = D\frac{\partial^2 u_3}{\partial x^2} - \gamma u_3, \quad x \in I_3 \tag{9}$$

We study this system at steady state. Imposing continuity boundary conditions yields a 4×4 linear system analogous to the 2×2 system solved in the one-sided case. The key

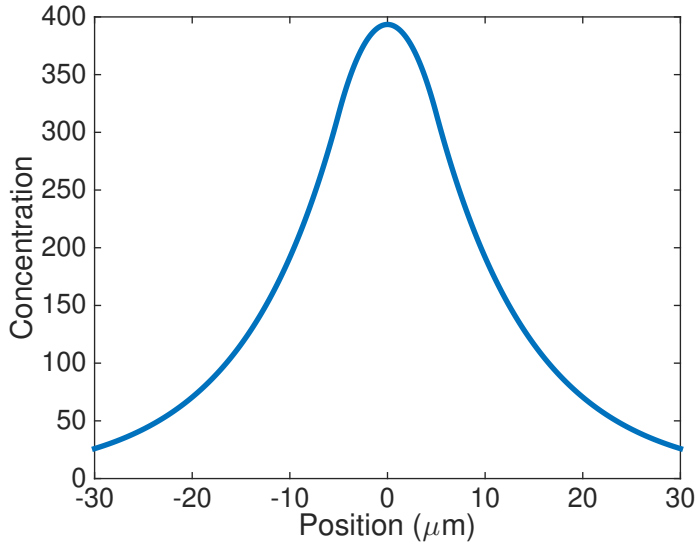

Figure S3: Plots of $u(x)$ in the symmetric case. Parameter values are $D = 1$, $\gamma = 0.01$, $L_s = 10$, and $\alpha = 10$.

parameter in all these results is the spatial correlation length, $\xi \equiv \sqrt{D/\gamma}$, along which the decay of the signal molecule produced by the sender strain occurs. Figure S1 shows that for $0 < L_s < \xi$, the density of signal felt at an area outside the stripe of sender cells increases as the thickness of the stripe increases. On the other hand, for $L_s > \xi$, there is not much change in the density of signal felt outside the stripe. Hence there is an optimal value for the thickness of the sender stripe, given by $L_s = \xi$, where a sender stripe can maximize its

range of influence at a minimal metabolic load. Figures S2 and S3 show that the decay of the spatial profile of the signal molecule occurs with a characteristic length scale given by ξ. This simple framework provides us with a means to look at several things. Namely, it gives an estimate to how far a receiver cell can be from a sender cell and respond to the signal molecule.

Supplementary Figures

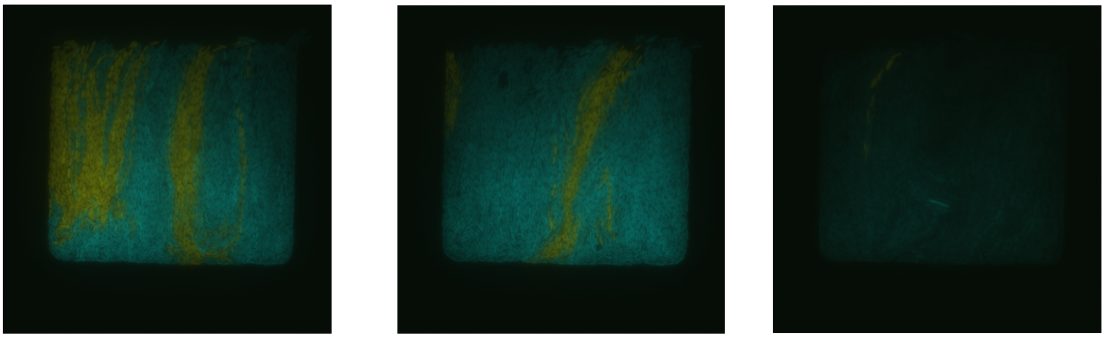

Figure S4: **Signaling in the small hallway trap.** Images of sender cells (yellow) cultured with receiver cells (cyan) over time in a hallway trap. Receiver cells fluoresce cyan in the presence of C4 HSL produced by sender cells. These images show that all receiver cells fluoresce cyan whenever there are sender cells present - up until the loss of sender cells in the trap in the rightmost image.

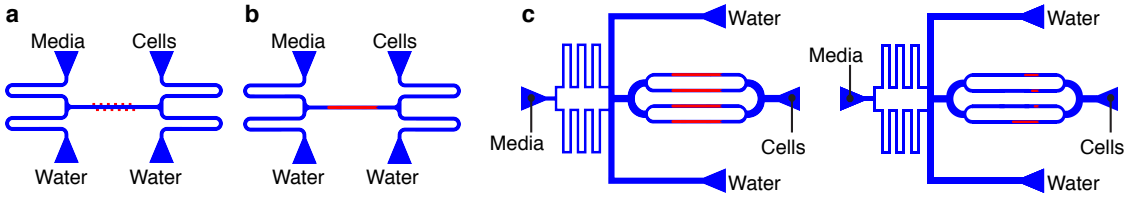

Figure S5: **Schematic of the entire microfluidic devices.** Blue regions are the 10 micron tall flow channel and the red regions are the cell-trapping regions. Blue triangle are ports to which media, cells, and waste reservoirs are connected. **(a)** The hallway trap device. Traps (red) are 1.5 microns tall. **(b)** The original (2mm) open trap device. Traps (red) are 0.95 microns tall. **(c)** The parallel device with four 2mm long open traps or with four different length traps: 1mm, 0.5mm, 0.225mm, and 0.1mm. Traps (red) are 0.95 microns tall.

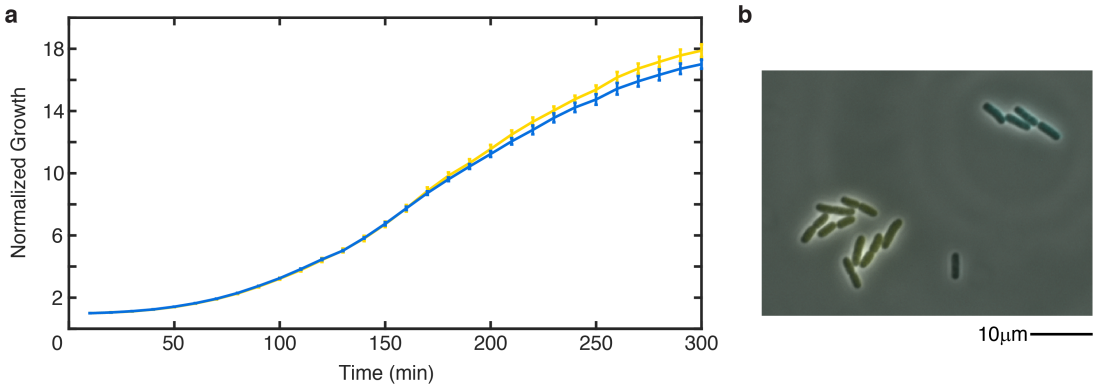

Figure S6: **Non-communicating strains have equal growth rates and sizes.** **(a)** Growth experiments in a 96-well plate over time show no significant difference in the growth rate of the two non-communicating strains. **(b)** Microscope images show similar size and shape of non-communicating strain in the fluidic devices.

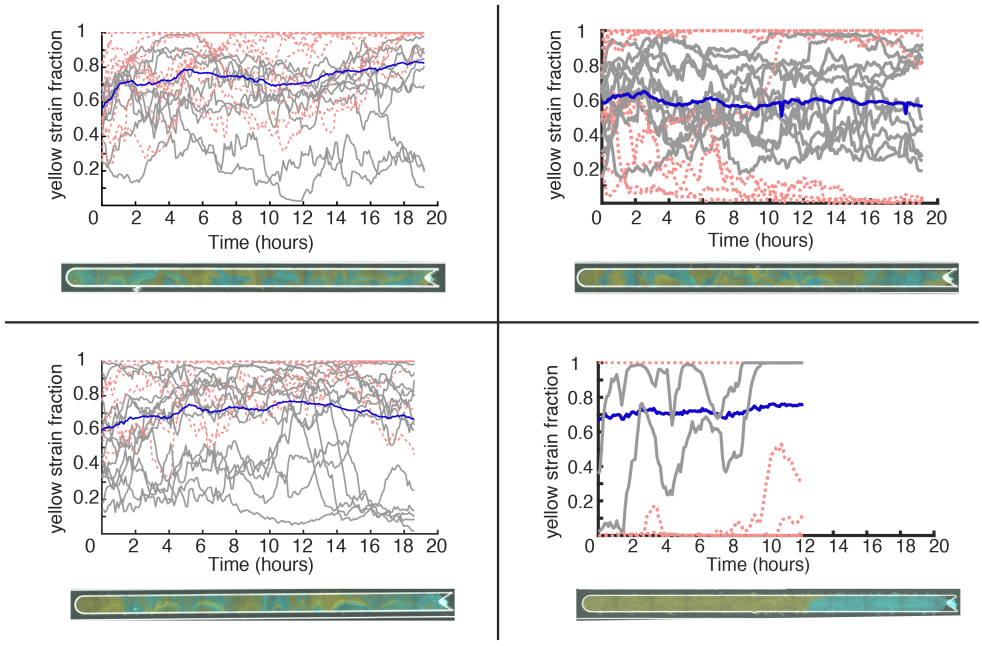

Figure S7: **Segmented open trap examples.** Data from four additional open traps when segmented. Image of each trap once filled with cells is shown below each graph. Blue lines are the entire trap yellow strain fraction; gray solid and red dashed lines are data from each hallway-length segment. Red dashed lines are segments that at some point lose one strain. All data looks noisy with hallway-like strain instability except the bottom right which shows a trap with only has about 2 bands of cell strains.

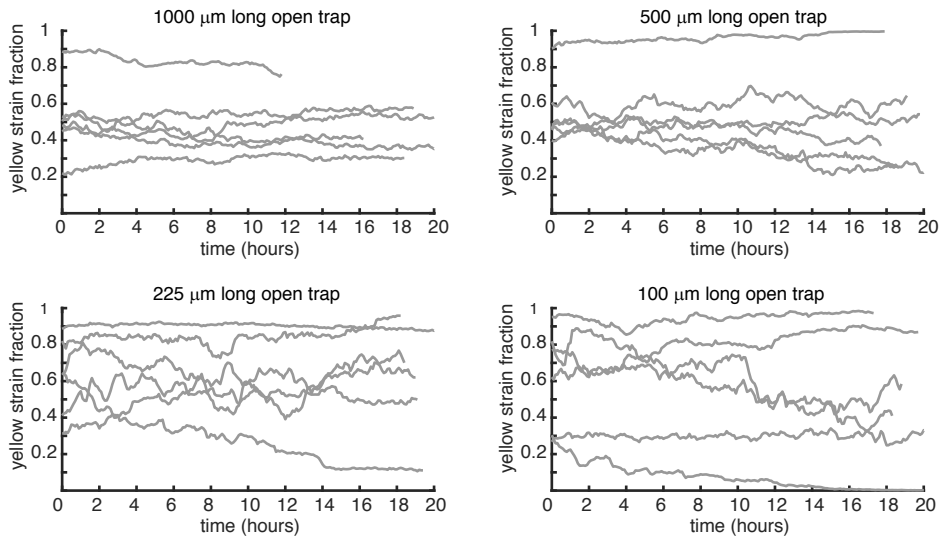

Figure S8: **Time Series from varied length traps.** Data of yellow strain fraction over time from each varied length trap experiment averaged in Fig. 4. As the open trap gets shorter, the strain ratios become more variable over time.

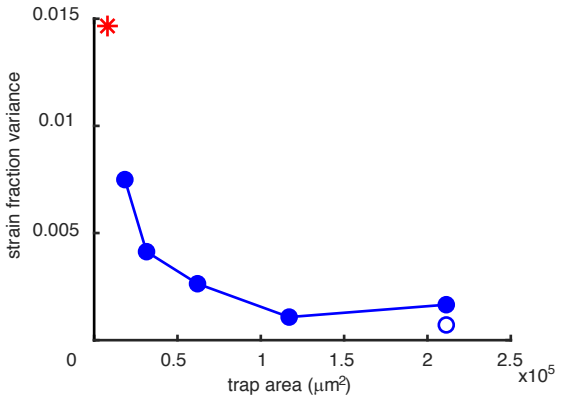

Figure S9: **Average strain ratio time series variance.** The variance of the yellow strain fraction over time is shown to compare with Fig. 4 in the main text, which plots the range of the yellow strain fraction. The two plots are qualitatively the same and show the trend of increased strain stability with increasing size of the cell-trapping area. Closed blue circles: average strain fraction variance of the open-walled devices of each trap size. The open circle for the longest open-walled device is lowered (open blue circle) when including only experiments with the 6 smallest number of resulting stripe bands (see main text and Fig. S10 and Fig. S11) Red star: same data but for the "hallway" device.

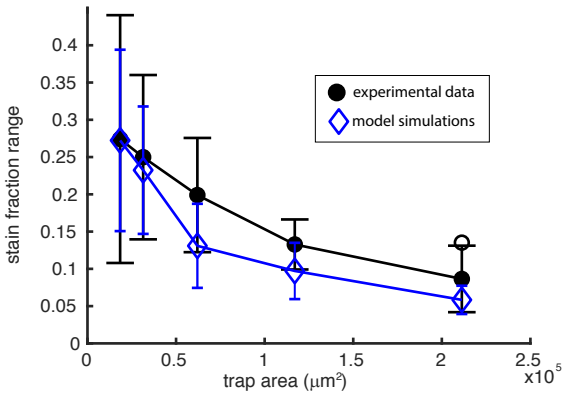

Figure S10: **Average strain fraction range vs. trap area for reduced data in the longest trap size: comparing model and experiment.** We reduced the experimental data set in the longest open-walled trap to compare with Fig. 4 in the main text. The reduced data reflect a similar number of striping bands as for the other trap sizes. Filled black circles: average yellow strain fraction range of the open-walled devices of each trap size (x-axis: cell-occupied trap area) with the last data point including the reduced data set only. Open black circle: Mean range while including all data for the longest trap size (same as in Fig. 4). The reduced data for the longest trap size support a conclusion that increased numbers of seed cells correlated with an increased number of measured striping bands in the experiment, which, in turn, correlated with measured strain ratio variability (our simulations support this claim, see Fig. S11). Model simulations interact strain band interfaces by seeding cells with a one-dimensional random placement and performing a random walk of the interface locations using a Poisson process of rate one to determine the step size. The single parameter of the model (the number of interactions per interface per simulated experiment hour) was set to fit the smallest trap size strain ratio range mean to that of the experiments. Compared to experiments, the simulations show a lower than measured strain ratio range for the larger trap and an overal higher experiment-to-experiment variability (error bars, $\pm$ one standard deviation from the mean), which we attribute to observed trap exit clogging and effects from hydrodynamic flow.

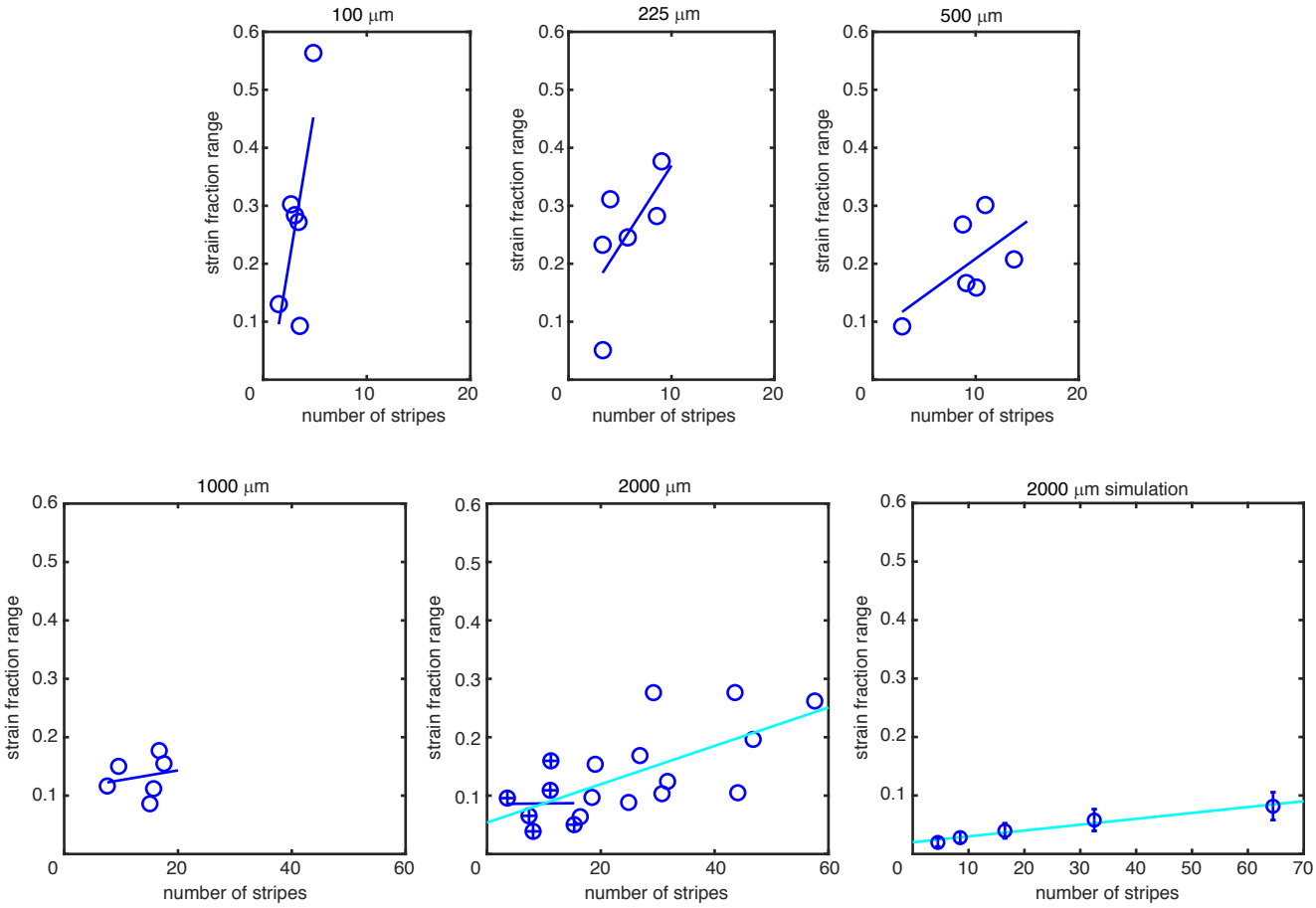

Figure S11: **Experimental strain fraction range vs. measured number of striping bands for each trap size.** Data for each length of open trap showing measured yellow strain fraction range vs. measured number of striping bands for each experiment in each device. Solid lines are linear least-squares fit of the data. In the 2000 μm length device, open blue circles show the entire data set, circles with filled + show the reduced data set, chosen to comprise the 6 data points with the smallest number of striping bands (thus, comparable to the data from other trap lengths). Blue line: least-squares linear fit to the reduced data. Cyan line: least-squares linear fit for the entire data set. In the last panel, we simulated the 2000 μm length device using a range of seed cell sizes that resulted in the number of initial bands shown. While we capture the trend of increasing strain ratio instability with increasing number of stripes in this size device, the simulated interactions from our simple modeling do not capture the strength of the interactions as measured in experiment. We attribute the differences to additional stochastic behavior, such as hydrodynamic flow and cell blockages that lead to spontaneous lateral cell flow, which are not captured by our simplistic interaction model. Seed cells were 8, 16, 32, 64, 128, which resulted in the expected number of initial stripes formed 4.5, 8.5, 16.5, 32.5, 64.5, respectively. Each simulated trap size was performed 10,000 times. Shown are mean strain fraction range and standard deviation with linear least-squares fit.

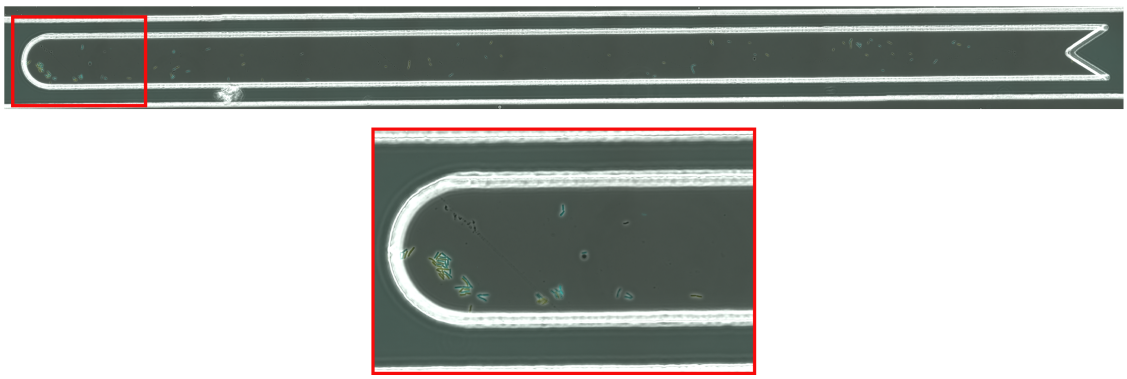

Figure S12: **Seeded cells clumped together.** This image is of the cells seeded into the last open trap from Fig. 5. As can be seen in the zoom in of the far left hand side of the trap, many cells have clumped together during the attempt to load a high number of cells into the trap. About 40 of the 123 cells seeded into the trap are in this small segment of the trap. Cells that are already clumped together when seeded will effectively act like one cell or colony and form one total band rather then each from their own band of cells when growing and filling the trap. We count touching cells of the same strain as one initial "colony" for the x-axis of Fig. 5.

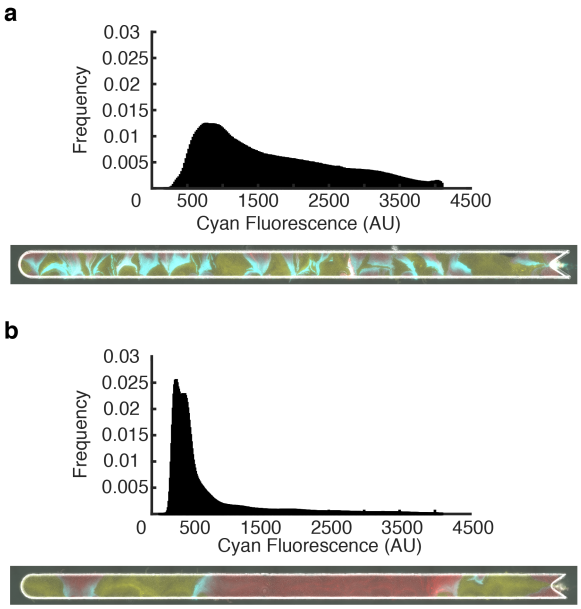

Figure S13: **Signalling in open trap.** **(a)** Distribution of CFP intensity of receiver cells in a well mixed open trap. All cells have fluorescence levels above background. **(b)** Distribution of CFP intensity of receiver cells in a less mixed open trap. Receiver cells further away from sender cells do not express significant levels of CFP.